

Information-Optimal Formation Geometry Design for Multimodal UAV Cooperative Perception

Kai Xiong, *Member, IEEE*, Xingyu Wu, Anna Duan, Supeng Leng, *Senior Member, IEEE*, Jianhua He, *Senior Member, IEEE*

Abstract—The efficacy of UAV swarm cooperative perception fundamentally depends on three-dimensional (3D) formation geometry, which governs target observability and sensor complementarity. In the literature, the exploitation of formation geometry and its impact on UAV sensing have rarely been studied, which can significantly degrade multimodal cooperative perception at scenarios where heterogeneous payloads (vision cameras and LiDAR) should be geometrically arranged to exploit their complementary strengths while managing communication interference and hardware budgets. To bridge this critical gap, we propose an information-theoretic optimization framework that allocation of UAVs and multimodal sensors, configures formation geometries, and flight control. The UAV-sensor allocation is optimized by the Fisher Information Matrix (FIM) determinant maximization. Under this framework we introduce an equivalent formation transition strategy that enhances field-of-view (FOV) coverage without compromising perception accuracy and communication interference. Furthermore, we design a novel Lyapunov-stable flight control scheme with logarithmic potential fields to generate energy-efficient trajectories for formation transitions. Extensive simulations demonstrate our formation-aware design achieves 25.0% improvement in FOV coverage, 104.2% enhancement in communication signal strength, and 47.2% reduction in energy consumption compared to conventional benchmarks. This work establishes that task-driven geometric configuration represents a foundational rather than incidental component in next-generation UAV swarm systems.

Index Terms—UAV 3D Formation, Multimodal Cooperative Perception, Fisher Information Matrix, Field-of-View.

I. INTRODUCTION

U Nmanned Aerial Vehicle (UAV) swarms have emerged as transformative platforms for cooperative perception, offering unprecedented capabilities in search and rescue (SAR), disaster response, and surveillance operations [1–3]. Unlike single-UAV systems or terrestrial sensor networks, swarms provide enhanced spatial coverage, improved viewpoint diversity, and parallel multimodal data acquisition through collaborative sensing [4]. Current literature predominantly focuses

on trajectory planning, resource allocation, and perception algorithms while treating the formation geometry of UAV swarms as a secondary implementation detail [5–10]. This oversight has significant impact on multimodal cooperative perception performance in scenarios where heterogeneous payloads (vision cameras and LiDAR) are strategically arranged to exploit their complementary strengths. Cameras provide rich visual semantics with low bandwidth requirements but suffer from depth estimation limitations, while LiDAR delivers precise 3D geometric information at the cost of higher communication overhead and energy consumption [11]. Without proper geometric configuration, these complementary sensing capabilities cannot be effectively leveraged, resulting in redundant observations, coverage gaps, and suboptimal target localization accuracy.

Despite these strong potentials, the efficacy of UAV swarm perception systems remains fundamentally constrained by their three-dimensional (3D) formation geometry, a critical factor that governs field-of-view (FOV) coverage, sensor complementarity, and target observability, yet is disproportionately overlooked in existing research. The challenge intensifies under practical operational constraints. In SAR missions, UAVs typically operate in close proximity, creating significant communication interference in dense formations [12]. While increasing swarm size enhances perception quality, it can significantly raise communication load, computational burden, and hardware costs. This requires a fundamental trade-off between perception performance and resource efficiency that cannot be resolved through conventional trajectory optimization alone. Furthermore, existing formation strategies typically assume homogeneous UAV capabilities [13, 14], without considering the spatial arrangement requirements of heterogeneous sensor payloads, which is a critical limitation for multimodal perception systems.

While significant progress has been achieved within each domain, existing research often treats these aspects in isolation, neglecting their intrinsic interdependencies. To bridge this critical gap, we propose an information-theoretic optimization framework that establishes formation geometry as a foundational design element for UAV swarm cooperative perception. This framework jointly optimizes spatial configuration, sensor heterogeneity, and perception performance through Fisher Information Matrix (FIM) determinant maximization. By treating formation design as a primary optimization variable rather than a byproduct of trajectory planning, we achieve simultaneous improvements in coverage completeness, communication Signal-to-Interference-plus-Noise Ratio (SINR), and flight en-

K. Xiong, X. Wu, and S. Leng are with School of Information and Communication Engineering, University of Electronic Science and Technology of China, Chengdu, 611731, China; and, Shenzhen Institute for Advanced Study, University of Electronic Science and Technology of China, Shenzhen, 518110, China.

A. Duan is with AVIC Chengdu Aircraft Design & Research Institute, 610041, Chengdu, 610041, China.

J. He is with School of Computer Science and Electronic Engineering, University of Essex, Colchester, UK.

The financial support of National Natural Science Foundation of China (NSFC), Grant No.62201122, and AVIC United Technology Center for Intelligent Decision-making and Coordinated Control Mechanism Model Research grant.

The corresponding author is Supeng Leng, email: spleng@uestc.edu.cn

ergy efficiency.

Specifically, this framework includes three sequential steps. First, we establish a novel FIM-based formation method that explicitly quantifies how spatial geometry and heterogeneous sensor placement influence cooperative perception performance. Second, we formulate and solve a formation transition problem that enhances FOV coverage while preserving perception quality and respecting practical constraints including directional FOV limitations and inter-UAV interference. Third, we develop a Lyapunov-stable distributed flight control strategy with logarithmic potential fields that guarantees energy-efficient formation transitions with bounded control authority. The main contributions of this paper are as follows:

- We establish a novel information-theoretic framework for 3D UAV swarm formation design that explicitly quantifies the interdependence between spatial geometry, heterogeneous sensor modalities, and cooperative perception performance. By leveraging FIM determinant maximization as the optimization criterion, our framework provides a principled approach to determine information-optimal formation configurations in versatile task environment where conventional homogeneous formation strategies fail to exploit multimodal sensing synergies.
- We formulate and solve a formation transition problem that addresses the FOV-oriented formation configuration under practical operational constraints. The proposed optimization model uniquely balances sensing information gain against FOV coverage completeness, communication overhead, and sensor payload costs. It incorporates realistic constraints including directional sensing limitations, inter-UAV interference effects, and heterogeneous payload capabilities that are typically neglected in existing literature.
- We develop a Lyapunov-stable distributed flight control strategy that guarantees energy-efficient formation transitions during dynamic operations. The control law employs a logarithmic potential field to ensure smooth trajectory generation with bounded control authority, provably minimizing unnecessary maneuvers and energy consumption while achieving asymptotic stability. Extensive simulations demonstrate that our integrated approach achieves significant improvements over conventional benchmarks in terms of localization accuracy, coverage robustness, and energy efficiency under both aerial and ground target search scenarios.

The remainder of this paper is organized as follows: Section II reviews related work. Section III presents our system architecture and problem formulation. Section IV details our optimization framework. Section V presents comprehensive simulation results, and Section VI concludes the paper.

II. RELATED WORK

This section reviews existing work in three interconnected research domains that collectively inform our formation-aware UAV cooperative perception framework.

A. UAV-based Search and Rescue

Recently there were increasing research and advances on the application of UAV swarm technologies for SAR. The SAR operations were classified into three categories in [15]: on-site monitoring and modeling, target perception and localization, and task allocation with path planning. Within on-site monitoring and modeling, Li *et al.* [16] proposed a cost-effective 3-D mapping methodology that generates precise survey point clouds through visual-inertial fusion. Tavakol Sadrabadi *et al.* [17] developed a multi-tiered swarm architecture specifically designed for wildfire emergency response, integrating fire detection and evacuation assistance capabilities. For target perception and localization, Xing *et al.* [18] introduced a vision-based cooperative framework leveraging YOLOv5 deep learning architecture to enable precise detection and localization of SAR targets across multiple UAV platforms.

In the areas of task allocation and trajectory planning, Zeng *et al.* [19] proposed the Differential Evolution-based Cooperative Search algorithm for multi-UAV systems, achieving a balance between coverage completeness and energy efficiency across diverse geographical terrains. Most recently, Yang *et al.* [20] introduced the Distributed Adaptive PSO algorithm, enhancing swarm responsiveness to dynamic environmental conditions during SAR operations. The above works advanced UAV swarm coordination and environmental awareness, but they mainly focus on temporal aspects of mission execution rather than spatial configuration optimization for perception enhancement.

B. Multimodal Cooperative Perception

Multimodal cooperative sensing has emerged as a critical technological advancement to overcome the inherent limitations of single-platform perception systems in terms of coverage breadth, accuracy, and environmental adaptability [21–23]. Within the UAV domain, Nitesh *et al.* [24] conducted an analysis of multimodal sensor integration techniques, demonstrating how EO/IR and radar system fusion can enhance detection precision, operational range, and overall system reliability in UAV applications. Their work showed that sensor complementarity can be exploited to outperform homogeneous sensing approaches across diverse operational conditions.

Several approaches are proposed to optimize multimodal perception. Tian *et al.* [25] introduced a framework employing multi-view geometry and feature fusion to enable collaborative 3D object detection across multiple UAVs, and mitigate perception blind spots caused by viewpoint variations. Similarly, Qiao *et al.* [26] proposed a dual-window cross-attention (DWCA) mechanism that integrates LiDAR and camera features into a unified Bird’s-Eye View representation, to improve perception performance through complementary modality fusion. Simon *et al.* [27] developed a real-time multimodal semantic reasoning architecture for UAV platforms, with on-line fusion of LiDAR, RGB, and thermal imaging data for enhanced environmental understanding. The development of standardized datasets has further accelerated research progress, with U2UData [28] establishing a benchmark featuring LiDAR

point clouds, RGB/depth images, environmental sensing measurements, and 3D annotations for investigating multi-UAV multimodal perception and communication strategies.

C. UAV Formation Design

UAV formations is critical for target localization, environmental monitoring, and critical surveillance applications. However, constrained by sensor precision and geometric configuration, determining optimal formation structures to enhance localization performance remains a pivotal challenge. The Fisher Information Matrix (FIM) and its associated metrics, particularly the Cramér-Rao Lower Bound (CRLB), have been employed to guide UAV formation design due to their ability to quantify theoretical limits of localization accuracy with mathematical rigor.

FIM analysis has been widely conducted for various localization techniques including time difference of arrival (TDOA), angle of arrival (AOA), received signal strength (RSS), and their hybrid configurations. Panwar *et al.* [13] integrated time of arrival (TOA), RSS, and AOA measurements, deriving the CRLB expression for joint measurements to evaluate target localization accuracy under realistic noise conditions. Similarly, Zhao *et al.* [14] transformed optimal placement problems for bearing-only, range-only, and RSS-based sensors into a unified parameter optimization framework, enabling cross-modal performance comparison. Hung *et al.* [29] proposed a heterogeneous sensing multi-UAV tracking system modeling hybrid measurement configurations incorporating image sensors, TOA, and AOA, employing the D-optimality criterion to design optimal UAV formation configurations that maximize information gain.

Regarding solution algorithms, Sahu *et al.* [30] developed a unified optimization framework integrating Alternating Direction Method of Multipliers (ADMM) with Majorization-Minimization techniques, for optimal sensor placements for source localization with provable convergence guarantees. Nakai *et al.* [31] proposed an efficient greedy optimization method tailored for different optimization criteria, to rapidly identify optimal sensor positions from large candidate sets while maintaining theoretical performance bounds. The above works developed a solid theoretical foundation for multimodal perception in UAV formation design.

Overall, current UAV swarm research disproportionately emphasizes trajectory planning and perception/communication frameworks while neglecting how 3D formation geometry fundamentally governs FOV coverage, sensor complementarity, and target observability. Furthermore, most formation design approaches assume homogeneous UAV capabilities, failing to leverage the synergistic potential of heterogeneous sensor payloads. Our work directly addresses this gap by introducing an information-theoretic optimization framework that holistically integrates these dimensions through FIM determinant maximization.

III. SYSTEM OPTIMIZATION FRAMEWORK

This section presents an architecture for UAV formation-based multimodal cooperative perception, structured around

three sequential strategies that collectively address the challenges of formation geometry, sensor heterogeneity, FOV coverage, and flight control. As shown in Fig. 1, the system follows a sequential optimization paradigm with three types of strategies. The UAV-sensor allocation strategy determines both the number of UAVs and the assignment of sensor category (LiDAR or Camera) to each UAV for optimal cooperative perception. The formation optimization strategy enhances FOV coverage while preserving cooperative perception and communication quality. The flight control strategy ensures energy-efficient flight trajectory to transfer the initial UAV swarm to the designated formation. This sequential approach holistically optimizes the geometric configuration, sensor complementarity, wireless communication, and flight energy.

A. System Assumption

The UAV formation for cooperative perception is demonstrated in Fig. 2, where heterogeneous UAVs collaboratively monitor an area for target detection and tracking. These UAVs equipped with complementary sensing modalities, some with image sensors (cameras) and others with point cloud sensors (LiDAR). The target, assumed to move on the ground or fly in the air, has a position given as $\mathcal{P}_{tar}(t) = [x_{tar}(t), y_{tar}(t), z_{tar}(t)]^T$. Each UAV i has a position $\mathcal{P}_i(t) = [x_i(t), y_i(t), z_i(t)]^T$ at time t . Assume that the pitch angle of the i -th UAV is 0° , then its heading vector is $\mathbf{b}_i = [\cos \theta_i, \sin \theta_i, 0]$ where θ_i represents the yaw angle of i -th UAV. The relative position between the i -th UAV and the target is:

$$\mathcal{P}_{i/tar}(t) = \mathcal{P}_i(t) - \mathcal{P}_{tar}(t). \quad (1)$$

Similarly, the relative position projected onto the X-Y plane is:

$$\mathcal{P}_{i/tar}^{xy}(t) = [x_i(t) - x_{tar}(t), y_i(t) - y_{tar}(t), 0]^T. \quad (2)$$

Subsequently, we will elaborate on the UAV-Sensor allocation, i.e., the formation configuration, for the multimodal cooperative perception.

B. Multimodal Cooperative Perception

This subsection explains multimodal cooperative perception in UAV swarms from information-theoretic perspective. Recognizing that heterogeneous sensor modalities offer complementary advantages in SAR scenarios, we develop a unified framework that quantifies perception performance using the FIM metric. This section analyzes two primary sensing modalities, the vision-based cameras and point-cloud-based LiDAR, deriving their respective measurement models, Jacobian matrices, and FIM formulations. We explicitly model the information contribution of each type of sensors within the formation aware framework. It can support optimal sensor allocation that maximizes target localization accuracy while accounting for practical constraints including FOV limitations, measurement noise characteristics, and communication interference effects.

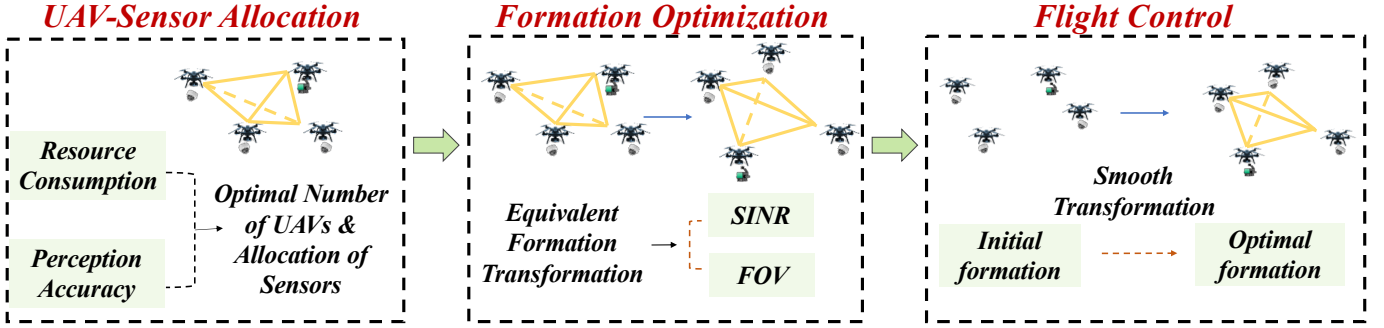


Fig. 1: The illustration of the comprehensive framework for the cooperative perception of UAV swarms.

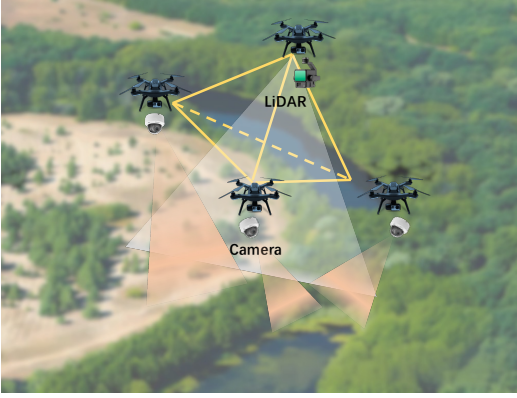


Fig. 2: UAV swarm-based SAR scenario.

1) *Perception Measurement of Camera*: Typically, the camera sensor maps the target position to the image pixel plane through a perspective projection way. The projection pixel coordinates $g_{\text{cam},i} = [u, v]^T$ is given as:

$$g_{\text{cam},i} = h_{\text{cam},i}(\mathcal{P}_{\text{tar}}, \mathcal{P}_i, \mathbf{n}_i) + \epsilon_{\text{cam}} \quad (3)$$

where ϵ_{cam} is measurement of image noise. It is related to the resolution level of the camera sensor and communication interference. In addition, h_{cam} is the projection function, which projects the target position to the camera coordinate system. It is defined as:

$$h_{\text{cam},i}(\mathcal{P}_{\text{tar}}, \mathcal{P}_i, \mathbf{n}_i) = \begin{bmatrix} u_i \\ v_i \end{bmatrix} = \pi \left[(R_g^c(\mathcal{P}_i - \mathcal{P}_{\text{tar}})) \right] \\ = \begin{bmatrix} -f_x \frac{\cos \theta_i (y_i - y_{\text{tar}}) - \sin \theta_i (x_i - x_{\text{tar}})}{\cos \theta_i (x_i - x_{\text{tar}}) + \sin \theta_i (y_i - y_{\text{tar}})} + c_x \\ -f_y \frac{z_i - z_{\text{tar}}}{\cos \theta_i (x_i - x_{\text{tar}}) + \sin \theta_i (y_i - y_{\text{tar}})} + c_y \end{bmatrix} \quad (4)$$

where R_g^c represents the rotation matrix from the global frame to the camera frame of i -th UAV. $\pi(\cdot)$ is a forward projection function that transforms a 3-D point from the camera frame to the pixel coordinates based on the intrinsic parameters of the camera. f_x and f_y are the focal lengths. Hereafter, the Jacobian matrix of the image measurement for the i -th UAV $O_{\text{cam},i}$ is given as:

$$O_{\text{cam},i} = \frac{\partial h_{\text{cam}}}{\partial \mathcal{P}_{\text{tar}}} \\ = \begin{bmatrix} \frac{-f_x (y_i - y_{\text{tar}})}{Z_i^2} & \frac{f_x (x_i - x_{\text{tar}})}{Z_i^2} & 0 \\ \frac{-f_y \cos \theta_i (z_i - z_{\text{tar}})}{Z_i^2} & \frac{-f_y \sin \theta_i (z_i - z_{\text{tar}})}{Z_i^2} & \frac{f_y}{Z_i} \end{bmatrix} \quad (5)$$

where $Z_i = \cos \theta_i (x_i - x_{\text{tar}}) + \sin \theta_i (y_i - y_{\text{tar}})$. Therefore, the FIM of the i -th UAV with a camera sensor is:

$$\mathcal{F}_{\text{cam},i} = O_{\text{cam},i}^T Q_{\text{cam}}^{-1} O_{\text{cam},i} \quad (6)$$

where Q_{cam} is the measurement covariance matrix, which is related to the pixel level of the camera and communication SINR.

2) *Perception Measurement of LiDAR*: The LiDAR sensor generates the point cloud data that can directly reflect the distance and three dimensional (3D) angle of the target. Accordingly, we can divide the perception measurement of LiDAR into a distance measurement and an angle measurement, respectively. For the distance measurement, it is:

$$d_i = h_d(\mathcal{P}_{\text{tar}}, \mathcal{P}_i) + \epsilon_d \quad (7)$$

where ϵ_d is the measurement noise and $h_d(\mathcal{P}_{\text{tar}}, \mathcal{P}_i)$ is the distance between the UAV i and target:

$$h_d(\mathcal{P}_{\text{tar}}, \mathcal{P}_i) = \sqrt{(x_i - x_{\text{tar}})^2 + (y_i - y_{\text{tar}})^2 + (z_i - z_{\text{tar}})^2} \quad (8)$$

Regarding 3-D angle measurement, it is comprised by the azimuth angle and the pitch angle of the target. The azimuth angle measurement β is expressed as:

$$\beta_i = h_A(\mathcal{P}_{\text{tar}}, \mathcal{P}_i) + \epsilon_A \quad (9)$$

where ϵ_A is the measurement noise and $h_A(\mathcal{P}_{\text{tar}}, \mathcal{P}_i)$ represents the azimuth angle difference, which is:

$$h_A(\mathcal{P}_{\text{tar}}, \mathcal{P}_i) = \tan^{-1} \left(\frac{y_i - y_{\text{tar}}}{x_i - x_{\text{tar}}} \right) \quad (10)$$

In contract, the pitch angle measurement δ is given as:

$$\delta_i = h_p(\mathcal{P}_{\text{tar}}, \mathcal{P}_i) + \epsilon_p \quad (11)$$

where ε_p is the noise and $h_p(\mathcal{P}_{tar}, \mathcal{P}_i)$ represents the pitch angle difference, which is:

$$h_p(\mathcal{P}_{tar}, \mathcal{P}_i) = \tan^{-1} \left(\frac{z_i - z_{tar}}{\sqrt{(x_i - x_{tar})^2 + (y_i - y_{tar})^2}} \right) \quad (12)$$

Based on the above analysis, the measurement of the LiDAR h_{lidar} is composed by:

$$h_{\text{lidar},i}(\mathcal{P}_{tar}, \mathcal{P}_i) = \begin{bmatrix} h_d(\mathcal{P}_{tar}, \mathcal{P}_i) \\ h_A(\mathcal{P}_{tar}, \mathcal{P}_i) \\ h_p(\mathcal{P}_{tar}, \mathcal{P}_i) \end{bmatrix} \quad (13)$$

Then, the Jacobian matrix $O_{\text{lidar},i}$ of the LiDAR measurement for i -th UAV is:

$$O_{\text{lidar},i} = \frac{\partial h_{\text{lidar}}}{\partial \mathcal{P}_{tar}} = \begin{bmatrix} -\frac{x_i - x_{tar}}{d_i} & -\frac{y_i - y_{tar}}{d_i} & -\frac{z_i - z_{tar}}{d_i} \\ \frac{\sin \beta_i}{d_i^{xy}} & -\frac{\cos \beta_i}{d_i^{xy}} & 0 \\ \frac{(z_i - z_{tar}) \cos \beta_i}{d_i^2} & \frac{(z_i - z_{tar}) \sin \beta_i}{d_i^2} & -\frac{d_i^{xy}}{d_i^2} \end{bmatrix} \quad (14)$$

where d_i^{xy} is the horizontal distance of the i -th UAV projected onto the tracking target, which is expressed as:

$$d_i^{xy} = \sqrt{(x_i - x_{tar})^2 + (y_i - y_{tar})^2}. \quad (15)$$

Finally, the FIM of LiDAR for i -th UAV is given as:

$$\mathcal{F}_{\text{lidar},i} = O_{\text{lidar},i}^T Q_{\text{lidar}}^{-1} O_{\text{lidar},i} \quad (16)$$

where Q_{lidar} is the measurement covariance matrix, which is related to the measurement and wireless transmission noise. Subsequently, we elaborate on the resource constraints of the communication interference, flight energy, and sensor budgets.

For mutually independent measurements, the total FIM is equal to the sum of the individual FIMs. Assuming the formation includes N_c camera-equipped UAVs and N_l LiDAR-equipped UAVs, and the sensor noises are mutually independent, the global FIM with respect to the target position, $\mathcal{F}_{\text{total}}$, can be expressed as:

$$\mathcal{F}_{\text{total}} = \sum_{i=1}^{N_c} \mathcal{F}_{\text{cam},i} + \sum_{j=1}^{N_l} \mathcal{F}_{\text{lidar},j} \quad (17)$$

C. Resource Consumption Analysis

1) *Signal-to-Noise Ratio*: Typically, the main communication between UAVs is the Line-of-Sight (LoS) link, in which only path loss is considered in the channel model. Thereby, the received signal power is:

$$p_{i_j}^{\text{rec}} = \rho_0 [(\mathcal{P}_j - \mathcal{P}_i)^2]^{\alpha/2} \quad (18)$$

where α is the path loss exponent, ρ_0 represents the path loss in free space at a distance of 1 meter [32]. \mathcal{P}_i is the position of i . Here, the signal-to-interference-plus-noise (SINR) of the

communication link between the i -th node and the j -th node is expressed as follows:

$$\eta_{ij} = \frac{p_{ij}^{\text{rec}}}{\sum_{k \in N, k \neq i, j} p_{kj}^{\text{rec}} + \sigma^2} \quad (19)$$

In the multimodal cooperative perception of the UAV swarm, the resource consumption mainly includes three aspects: communication consumption, flight maneuver energy consumption, and the inherent costs of heterogeneous sensors. Quantitative analysis of these costs is crucial for evaluating the feasibility of the system and optimizing the overall efficiency.

2) *Time-Frequency Communication Resource*: Regarding the i -th UAV, the time-frequency resource block for transmitting sensing data can be expressed as:

$$\mathcal{E}_i^{\text{comm}} = B_i \cdot T_i \quad (20)$$

where B_i is the occupied bandwidth for i -th UAV's data transmission. T_i represents the corresponding transmission duration for i -th UAV's, which can be regarded as the wireless channel occupation time. Due to the inherently larger data volume of LiDAR-based point clouds compared to RGB images, LiDAR-equipped UAVs generally incur higher time-frequency resource block consumption with the prescribed transmission rate.

3) *Sensor Hardware Budgets*: Multimodal sensors incur distinct operational and manufacturing budgets. The hardware cost C^{sensor} of onboard UAV sensors can generally be considered as a constant. Additionally, the hardware cost C_i^{lidar} of LiDAR is higher than those of cameras C_i^{cam} . Thus, there is $C_i^{\text{lidar}} > C_i^{\text{cam}}$.

D. Properties of FIM

To facilitate the analysis, the feasible position set for the UAVs is modeled as a finite discrete space \mathcal{V} , from which a subset of positions is selected to configure the UAV swarm. The objective function, denoted as $f(S)$, is formulated to maximize the FIM (or a scalar metric thereof, such as the log-determinant). To guarantee that the proposed strategy yields an optimal solution, $f(S)$ is required to satisfy two fundamental properties: *monotonicity* and *submodularity*.

Monotonicity: For any two subsets S and T satisfying $S \subseteq T \subseteq V$, the following inequality holds:

$$f(T) \geq f(S). \quad (21)$$

This property implies that adding an additional UAV to an existing sub-swarm will not degrade the collaborative sensing performance.

Submodularity: For any two subsets S and T with $S \subseteq T \subseteq V$, and for any new candidate position $v \in V \setminus T$, the function $f(\cdot)$ exhibits the property of diminishing returns, defined as:

$$f(S \cup \{v\}) - f(S) \geq f(T \cup \{v\}) - f(T). \quad (22)$$

This inequality indicates that the marginal gain in estimation precision achieved by adding a new UAV v is greater (or equal) when added to a smaller subset S than to a larger subset T .

The monotonicity and submodularity of $f(\cdot)$ guarantee that a greedy strategy yields a computationally efficient solution with a lower-bound performance guarantee of $(1 - 1/e) \approx 63.2\%$ relative to the optimal solution [31].

IV. FORMATION AWARE STRATEGIES

To address the cooperative perception problem, including sensing performance, communication, and flight energy constraint, we divide the UAV formation scheme into three sub-problems: the UAV-sensor allocation, FOV-oriented formation optimization, and energy-efficient flight control.

A. UAV-Sensor Allocation

The first subproblem aims to determine the optimal number of UAVs and the multimodel sensor allocation (camera and LiDAR) within the swarm. The objective is to maximize the collaborative sensing accuracy for target tracking, while considering the diminishing reward of new node incorporation and the associated costs of communication overhead and hardware deployment.

We adopt the D-optimality (Determinant-optimality) criterion from optimal experimental design, which leads to the following objective function [33]:

$$f(U) = \log \det \mathcal{F}(U), \quad (23)$$

where $U \subseteq V$ denotes the selected subset of UAVs from the candidate set \mathcal{V} , and $\mathcal{F}(U)$ represents the FIM for the selected configuration. Crucially, the log-determinant of the FIM has been rigorously proven to satisfy both monotonicity and submodularity [33, 34], thereby validating the theoretical applicability of the proposed greedy selection strategy.

To balance sensor performance of different UAVs with practical resource constraints, we augment the objective with penalty terms for communication time-frequency resource and hardware costs:

$$\mathcal{J}(U) = \log \det \mathcal{F}(U) - \alpha_1 \sum_{v \in U} \mathcal{E}_v^{\text{comm}} - \alpha_2 \sum_{v \in U} C_v^{\text{sensor}}, \quad (24)$$

where $\mathcal{E}_v^{\text{comm}}$ quantifies the time-frequency resources block of UAV v , C_v^{sensor} represents the sensor hardware costs, and α_1, α_2 are weighting coefficients that regulate the trade-off between detection performance and resource utilization according to the task requirements. Based on the above analysis, we present the optimization model for UAV cooperative perception:

$$\begin{aligned} \text{(P1): } & \max_{U \subseteq V} \mathcal{J}(U) \\ \text{s.t. } & C_1 : |U| \leq N_{\max} \\ & C_2 : d_{\min} \leq d_v \leq d_{\max}, \quad \forall v \in U \\ & C_3 : \beta_{\min} \leq \beta_v \leq \beta_{\max}, \quad \forall v \in U \\ & C_4 : \delta_{\min} \leq \delta_v \leq \delta_{\max}, \quad \forall v \in U \\ & C_5 : s_v \in \{\text{Camera, LiDAR}\}, \quad \forall v \in U, \end{aligned} \quad (25)$$

in which C_1 is the maximum number of deployed UAVs according to practical conditions and coordination capabilities.

C_2 gives the distance range constraints, designed to ensure a safe separation from the target while simultaneously keeping the UAV within the sensor's effective perception coverage. C_3 and C_4 specify the azimuth and pitch angle constraints, respectively, guaranteeing that the target remains within the sensor's effective FOV. And C_5 represents the available sensor category, i.e., the camera and LiDAR.

Notably, the monotonicity and submodularity properties of the FIM enable us to employ efficient greedy selection algorithms with theoretical optimal value guarantees. The marginal gain of incorporating an additional UAV v into an existing set U_j which contains j number of UAVs is defined as:

$$\Delta(v|U_j) = f(U_j \cup v) - f(U_j) \quad (26)$$

Moreover, to implement the greedy selection algorithm, we introduce an utility function that incorporates both marginal gains and system costs:

$$G(v) = \Delta(v|C_j) - \alpha_1 \mathcal{E}_v^{\text{comm}} - \alpha_2 C_v^{\text{sensor}} \quad (27)$$

The core of our greedy selection strategy involves iteratively choosing UAV spatial configurations from a finite candidate set \mathcal{V} , constructed through discretization of the solution space encompassing all feasible UAV positions and sensor combinations. Specifically, the candidate set V is constructed as follows:

Spatial Discretization: We model the 3D airspace surrounding the target using a spherical coordinate system centered at the target's estimated position. The radial distance d is discretized at intervals Δd within $[d_{\min}, d_{\max}]$, bounded by the effective sensing range of onboard sensors. Similarly, the azimuth angle β and pitch angle δ are uniformly sampled at resolutions $\Delta\beta$ and $\Delta\delta$, respectively, ensuring comprehensive coverage of possible observation directions. This discretization yields a structured grid of spatial candidate points $p_{\text{candidate}} = (d, \beta, \delta)$.

Sensor Assignment: For each spatial candidate position, we generate two distinct UAV-sensor configurations: one equipped with a camera sensor and another with a LiDAR sensor. This explicit incorporation of sensor heterogeneity doubles our candidate set size but enables optimal sensor modality selection based on information contribution and hardware constraints.

View Direction: We analytically determine the optimal yaw orientation θ_i by aligning the sensor's optical axis directly toward the target. This geometric constraint maximizes perceptual quality while reducing the search space dimensionality, as the yaw angle becomes a deterministic function of the relative position between UAV and target rather than an independent optimization variable.

Algorithm 1 summarizes the complete greedy selection procedure. The algorithm terminates when the maximum utility gain $G(v_t)$ falls below a predefined threshold ρ , indicating that additional UAVs no longer justify their associated communication and hardware costs. This termination criterion, combined with the submodular property of our objective function, guarantees a $(1 - 1/e)$ -approximation to the optimal

solution while maintaining computational efficiency through linear complexity $\mathcal{O}(|V|)$, making it suitable for real-time swarm configuration in time-critical SAR operations.

Algorithm 1: Greedy Selection for Optimal UAV-Sensor Configuration

```

1 Input: Candidate set  $V$ , cost coefficients  $\alpha_1, \alpha_2$ ,
   time-frequency resource  $\mathcal{E}$ , sensor hardware budgets
    $C^{sensor}$ , termination threshold  $\rho$ 
2 Output: Optimal UAV-sensor configuration  $U_M$ 
3  $U_0 \leftarrow \emptyset$ ;  $M \leftarrow 0$ 
4 while true do
5    $M \leftarrow M + 1$ 
6   for each  $v \in V \setminus U_{M-1}$  do
7      $\Delta(v|U_{M-1}) \leftarrow$ 
        $\log \det \mathcal{F}(U_{M-1} \cup v) - \log \det \mathcal{F}(U_{M-1})$ 
8      $G(v) \leftarrow \Delta(v|U_{M-1}) - \alpha_1 \mathcal{E}_v^{comm} - \alpha_2 C_v^{sensor}$ 
9    $v_t \leftarrow \arg \max_{v \in V \setminus U_{M-1}} G(v)$ 
10  if  $G(v_t) \leq \rho$  then
11    break
12   $U_M \leftarrow U_{M-1} \cup \{v_t\}$ 
13 return  $U_M$ 

```

B. Formation Optimization

Having determined the optimal UAV-sensor configuration through the Alg. 1, we now address the optimal spatial formation to maximize the FOV coverage without FIM loss. While the selected UAVs and sensors provide theoretically optimal target localization accuracy, their initial geometric configuration may exhibit significant FOV gaps and communication interference that compromise operational robustness in dynamic SAR scenarios. This subsection introduces an equivalent transformation framework that preserves the fundamental perception accuracy (the FIM determinant) while strategically reconfiguring UAV positions to maximize FOV coverage completeness and communication quality.

To ensure continuous target tracking during surveillance operations, FOV coverage constitutes a critical performance metric beyond mere perception accuracy. An optimal formation must not only maintain target observability but also provide spatially balanced observation perspectives to mitigate occlusion risks and accommodate potential target maneuvers. We model each UAV's FOV coverage as a rectangular pyramidal frustum determined by three geometric parameters: maximum perception range d_{\max} , horizontal FOV (HFOV) γ , and vertical FOV (VFOV) κ . Fig 3 presents the pyramidal frustum-based FOV demonstration.

Given our assumption that all UAVs maintain direct orientation toward the target, the visibility constraint simplifies to a combined distance and angular verification: the target must satisfy $d_i \leq d_{\max}$ while simultaneously falling within the angular boundaries defined by γ and κ . To quantify coverage quality, we discretize the spherical space surrounding the target into \mathcal{N} equally spaced azimuth directions represented by unit vectors $\mathbf{n}_k = [\cos \phi_k, \sin \phi_k, 0]^T$, where $\phi_k = 2\pi k/\mathcal{N}$ for

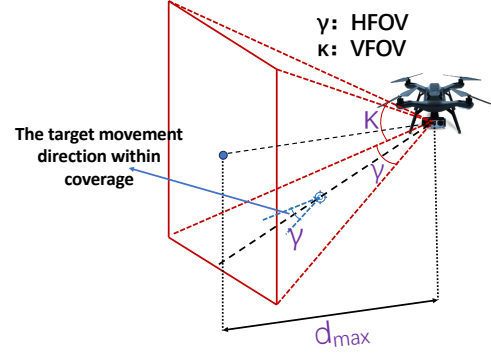


Fig. 3: Demonstration of Field of View.

$k = 0, 1, \dots, \mathcal{N} - 1$. A direction \mathbf{n}_k is considered covered if at least one UAV i satisfies:

$$\arccos \left(\frac{\mathbf{n}_k \cdot \mathcal{P}_{i/tar}^{xy}}{\|\mathcal{P}_{i/tar}^{xy}\|} \right) \leq \frac{\gamma_i}{2} \quad (28)$$

where $\mathcal{P}_{i/tar}^{xy}$ denotes the horizontal component (x-y plane) of the relative position vector between UAV i and the target. For each direction \mathbf{n}_k , we define a coverage intensity metric:

$$\Phi(\mathbf{n}_k) = \sum_{j=1}^M \frac{\mathbb{I}_{j/k}}{1 + \lambda \|\mathcal{P}_{j/tar}^{xy}\|} \quad (29)$$

where $\mathbb{I}_{j/k}$ is an indicator function is an indicator function equal to 1 if direction \mathbf{n}_k is covered by UAV j , and 0 otherwise, while λ represents a distance-weighting factor and M is the number of UAVs obtained from Alg. 1. To penalize uncovered directions and promote coverage integrity, we introduce a penalty term ξ :

$$\xi = 1 - \frac{\mathcal{N}_{\text{uncovered}}}{\mathcal{N}} \quad (30)$$

where $\mathcal{N}_{\text{uncovered}} = \sum_{k=1}^{\mathcal{N}} \mathbb{I}(C(\mathbf{n}_k) = 0)$ denotes the count of uncovered directions. The comprehensive FOV coverage metric Γ combines these elements:

$$\Gamma = \xi * \sum_{k=0}^{\mathcal{N}-1} \Phi(\mathbf{n}_k) \quad (31)$$

Given the optimal UAV set U_M from Alg. 1, we formulate the formation optimization problem to maximize FOV coverage while preserving perception performance. Crucially, we leverage the property that equivalent geometric transformations (particularly UAV flips about the target) maintain the determinant of the FIM unchanged while altering the formation geometry [14]. This insight enables us to search within an equivalence class of formations that guarantee identical estimation accuracy but potentially superior FOV coverage characteristics with wireless transmission constraints. The optimization problem is formally stated as:

$$(P2): \quad \max_{\mathcal{P}_i \in U_M} \Gamma \quad (32)$$

$$\text{s.t.} \quad \eta^{\text{SINR}} \geq \eta_{\min}^{\text{SINR}}$$

where $\eta_{\min}^{\text{SINR}}$ represents the minimum required SINR ratio for reliable wireless communication.

To address the combinatorial complexity of evaluating all 2^M possible flip configurations for M UAVs, we develop an efficient search strategy based on azimuth sector partitioning. The algorithm first computes the yaw angle θ_i of each UAV with respect to the target. Since each UAV is assumed to face the target, the yaw angle is determined by the bearing from the UAV to the target:

$$\theta_i = \text{atan2}(y_{\text{tar}} - y_i, x_{\text{tar}} - x_i). \quad (33)$$

where $\text{atan2}(y, x)$ denotes the two-argument arctangent function, which returns the angle of the vector (x, y) in the full range $(-\pi, \pi]$ and correctly handles all quadrants. These angles are then partitioned into K sectors according to

$$\text{sector}_i = \lfloor \frac{\theta_i}{2\pi/K} \rfloor \quad (34)$$

Within sectors containing multiple UAVs (typically exhibiting high coverage overlap), we prioritize flipping operations for UAVs that yield the greatest marginal improvement in Γ while satisfying the SINR constraint.

Alg. 2 details this formation optimization procedure, which systematically evaluates candidate flips while pruning the search space through sector-based constraints. This approach efficiently identifies the UAV formation that maximize FOV coverage completeness without compromising perception accuracy or communication reliability.

Algorithm 2: FOV-oriented Formation Optimization

```

1 Input: Initial formation  $U$  from Alg. 1, target position
    $\mathbf{p}_t$ , minimum SINR threshold  $\eta_{\text{SINR}}^{\min}$ , number of
   azimuth sectors  $K$ 
2 Output: Optimized formation  $U^*$ 
3  $U^* \leftarrow U$ ,  $\mathcal{F}^* \leftarrow \Gamma(U)$ 
4 for each  $u_i \in U$  do
5    $\theta_i \leftarrow \text{atan2}(y_{\text{tar}} - y_i, x_{\text{tar}} - x_i)$ ,
6    $\text{sector}_i \leftarrow \lfloor \frac{\theta_i}{2\pi/K} \rfloor$ 
7 for each sector $_k$  with multiple UAVs do
8   for each  $u_i \in \text{sector}_k$  do
9      $U' \leftarrow \text{Flip}(U, u_i)$ ,
10     $\mathcal{F}' \leftarrow \Gamma(U')$ 
11    if  $\eta^{\text{SINR}}(U') \geq \eta_{\text{SINR}}^{\min}$  and  $\mathcal{F}' > \mathcal{F}^*$  then
12       $U^* \leftarrow U'$ 
13       $\mathcal{F}^* \leftarrow \mathcal{F}'$ 
14 return  $U^*$ 

```

C. Flight Trajectory Control

Building upon the optimal FOV formation derived in Section IV-B, this subsection addresses the challenge of transitioning the UAV swarm from its initial position to the desired geometric formation $\mathcal{P}^* = [\mathcal{P}_1^*, \mathcal{P}_2^*, \dots, \mathcal{P}_m^*]^T$ while ensuring energy efficiency, trajectory smoothness, and asymptotic stability. Rather than employing conventional control approaches

that often prioritize rapid convergence at the expense of energy consumption and maneuver aggressiveness, we develop a Lyapunov-based distributed control framework that systematically balances formation accuracy with operational efficiency. The proposed control architecture incorporates a logarithmic potential field to bound control authority during large formation errors, thereby preventing excessive maneuvers while guaranteeing global asymptotic stability.

At the beginning, we model each UAV's dynamics using a double integrator system:

$$\dot{\mathcal{P}}_i(t) = v_i(t) \quad (35)$$

$$m_i \dot{v}_i(t) = u_i(t) \quad (36)$$

where \mathcal{P}_i , v_i , and m_i represent the position, velocity, and mass of the i -th UAV, respectively, and $u_i(t)$ denotes the control input. Additionally, the desired formation is characterized by target relative displacements d_{ij} between neighboring UAV pairs (i, j) , satisfying $\mathcal{P}_i^* - \mathcal{P}_j^* = d_{ij}$ where $d_{ij} = -d_{ji}$. Then, the formation error between UAVs i and j is defined as:

$$\mathbf{e}_{ij}(t) = \mathcal{P}_i(t) - \mathcal{P}_j(t) - d_{ij} \quad (37)$$

where \mathcal{P}_i^* indicates the desired position of the i -th UAV. The formation objective requires $\mathbf{e}_{ij} \rightarrow 0$ for all connected pairs. The communication topology is represented by a connected undirected graph \mathcal{G} , with \mathcal{M}_i denoting the neighbor set of UAV i .

We implement a leader-follower architecture where a designated leader UAV L incorporates trajectory tracking capability while follower UAVs execute distributed formation control. The control law for the leader UAV is designed as:

$$\mathbf{u}_L = -k_1 \sum_{j \in \mathcal{M}_L} \frac{\mathbf{e}_{Lj}}{1 + \|\mathbf{e}_{Lj}\|^2} - k_2 \mathbf{v}_L - k_p (\mathcal{P}_L - \mathcal{P}_L^{\text{des}}) \quad (38)$$

where $\mathcal{P}_L^{\text{des}}$ represents the leader's desired absolute position (determined by the tracked target's current location), and $k_1, k_2, k_p > 0$ are control gains. For follower UAVs ($i \neq L$), the control law is:

$$\mathbf{u}_i = -k_1 \sum_{j \in \mathcal{M}_i} \frac{\mathbf{e}_{ij}}{1 + \|\mathbf{e}_{ij}\|^2} - k_2 \mathbf{v}_i \quad (39)$$

The stability of the closed-loop system is established using Lyapunov theory. Consider the candidate Lyapunov function:

$$\mathcal{V} = \sum_{(i,j) \in \mathcal{G}} \ln(1 + \|\mathbf{e}_{ij}\|^2) + \sum_i \frac{1}{2} \|\mathbf{v}_i\|^2 + \alpha \|\mathcal{P}_L - \mathcal{P}_L^{\text{des}}\|^2. \quad (40)$$

This positive definite function combines three key components: (i) a logarithmic potential field $\ln(1 + \|\mathbf{e}_{ij}\|^2)$ that bounds control authority during large formation errors, preventing excessive maneuvers; (ii) a velocity damping term $\|\mathbf{v}_i\|^2$ that suppresses oscillations and ensures smooth velocity profiles; and (iii) a trajectory tracking component $\alpha \|\mathcal{P}_L - \mathcal{P}_L^{\text{des}}\|^2$ for the leader UAV L . Together, these elements synergistically balance convergence speed with energy

efficiency while guaranteeing formation accuracy. Hereafter, differentiating Eq. (40) with respect to time yields:

$$\dot{\mathcal{V}} = \sum_{i=1}^M \left(\sum_{j \in \mathcal{M}_i} \frac{2\mathbf{e}_{ij}}{1 + \|\mathbf{e}_{ij}\|^2} \right)^T \mathbf{v}_i + \sum_{i=1}^M \mathbf{v}_i^T \mathbf{u}_i + \alpha(\mathcal{P}_L - \mathcal{P}_L^{\text{des}})^T \mathbf{v}_L \quad (41)$$

Substituting the control law (Eq. (38) and (39)) into the system dynamic (Eq. (41)) with $k_1 = 4$, $k_p = \alpha$, we obtain:

$$\dot{\mathcal{V}} = -k_2 \sum_{i=1}^M \|\mathbf{v}_i\|^2 \leq 0 \quad (42)$$

By LaSalle's invariance principle [35], the system is globally asymptotically convergence, ensuring all UAVs converge to their designated positions in the desired formation. The logarithmic potential field in the Lyapunov function specifically optimizes trajectory smoothness by preventing control saturation during large formation errors, thereby minimizing energy-intensive maneuvers while maintaining precise formation tracking. This design achieves an optimal balance between formation accuracy, trajectory smoothness, and energy efficiency for UAV swarm operations.

V. NUMERICAL SIMULATION

This section presents a comprehensive numerical validation of the proposed UAV formation framework across three critical dimensions: UAV-sensor allocation optimization, FOV-oriented formation geometry enhancement, and energy-efficient flight control. Building upon the proposed framework and algorithms presented in Sections III and IV, we implement a multi-faceted evaluation methodology that quantifies performance improvements against conventional benchmarks while respecting practical constraints including communication interference, energy limitations, and hardware budgets. The simulation environment integrates wireless communication models, sensor measurement characteristics, and flight dynamics to provide rigorous validation under different conditions. Tab. I summarizes the key simulation parameters used throughout our experimental analysis.

TABLE I: Simulation parameters

| | |
|--|---------------------------------|
| path loss exponent α | 2.0 |
| noise power σ^2 | -110 dBm |
| camera focal lengths $f_x = f_y$ | 381.0 pixels |
| LiDAR covariance matrix Q_{lidar} | $\text{diag}(0.1, 0.02, 0.015)$ |
| camera covariance matrix Q_{cam} | $\text{diag}(6, 6)$ |
| HFOV γ | 50° |
| VFOV κ | 40° |

A. UAV-Sensor Allocation

We implemented the proposed greedy algorithm detailed in Section IV-A to determine the optimal configuration of UAVs and sensor modalities. The objective function maximizes $\log \det \mathcal{F}(C)$, while incorporating penalty terms for time-frequency resource consumption $\mathcal{E}^{\text{comm}}$ and hardware

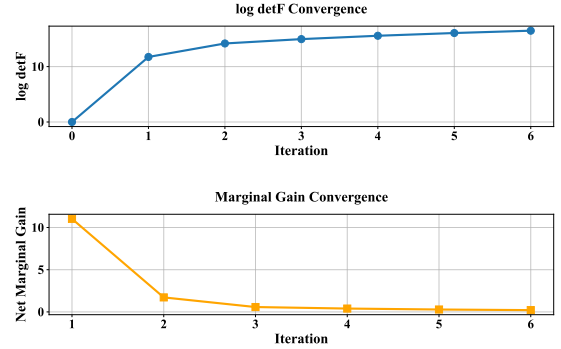


Fig. 4: Formation perception accuracy and marginal gain.

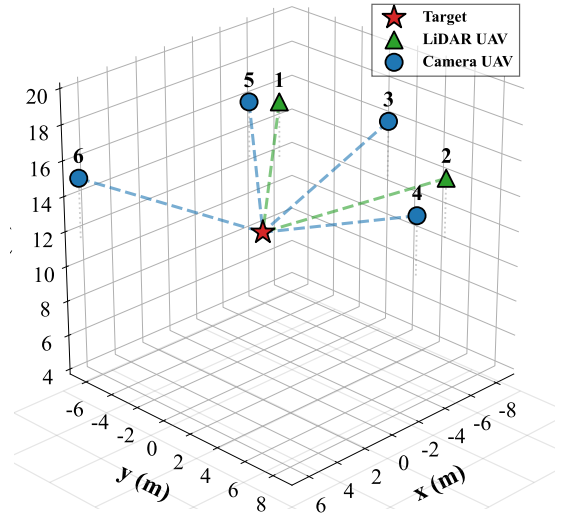


Fig. 5: 3D heterogeneous UAV formation configuration.

budgets C^{sensor} . The weighting coefficients were set to $\alpha_1 = 0.18$, $\alpha_2 = 0.2$ with the termination threshold $\rho = 0.17$ for simulation.

Fig. 4 presents the convergence of the optimization process. As expected from the submodular property of the FIM determinant, the perception accuracy diminishing returns as additional UAVs are incorporated into the UAV formation. This result validates our theoretical analysis and justifies the termination criterion for the greedy algorithm (Alg. 1). The optimization identifies an optimal configuration comprising six UAVs (four camera-equipped and two LiDAR-equipped units) that achieves a good balance between perception accuracy and system cost. The corresponding formation geometry and sensor distribution are visualized in Fig. 5, with detailed parameters provided in Tab. II.

Fig. 6 provides the performance comparison between multimodal and single-modal formation by applying the same proposed greedy selection algorithm, in which the multimodal containing camera and LiDAR; the single-modal refers to carrying only a camera or LiDAR. The result shows that the proposed multimodal strategy achieves superior perception accuracy. Specifically, the optimized multimodal UAV formation attains a $\log \det(\mathcal{F})$ value of 16.48, whereas the LiDAR-only

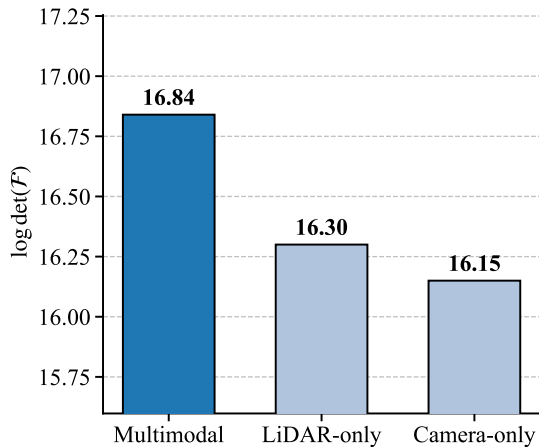


Fig. 6: Performance comparison between multimodal and single-modal formation.

configuration yields a $\log \det(\mathcal{F})$ of 16.30 using 4 LiDAR-equipped UAVs. In contrast, the camera-only configuration achieves a $\log \det(\mathcal{F})$ of 16.15 with 7 camera-equipped UAVs. These results highlight that multimodal perception not only enhances collaborative performance but also achieves this with a more efficient allocation of UAV-sensor resources. In that the multimodal formation only requires 6 UAVs where 2 UAV carrying LiDAR and 4 UAV carrying camera).

To assess the effectiveness of our greedy selection algorithm, we conducted a comparative analysis against the global optimum obtained through exhaustive search over all possible configurations with identical sensor composition (two LiDAR and four camera-equipped UAVs). The greedy algorithm achieved a $\log \det$ FIM value of 16.482 compared to the global optimum of 19.884, satisfying the theoretical $(1 - 1/e)$ -approximation guarantee. Furthermore, as demonstrated in Fig. 7, our approach locates a near-optimal solution within 0.56 seconds, significantly outperforming the Monte Carlo baseline method which requires substantially greater computational resources to achieve comparable performance. This efficiency stems from the reduction in computational complexity from combinatorial $\mathcal{O}(|V|^K)$ to linear $\mathcal{O}(K \cdot |V|)$, confirming the algorithm’s suitability for real-time applications.

To analyze the sensitivity to discretization precision, we conducted comparative experiments with varying angular resolution parameters. As shown in Fig. 8, the discretization granularity significantly impacts FIM determinant values. Coarse discretization (e.g., $\beta = 60, \delta = 30$) fails to identify optimal configurations, resulting in degraded perception accuracy. Moderate precision settings (e.g., $\beta = 10, \delta = 10$) achieve an optimal balance between computational efficiency and solution quality. Notably, pitch angle discretization demonstrates greater influence on accuracy than azimuth discretization, providing practical guidance for parameter selection in real-world implementations.

B. FOV-oriented Formation Performance

Building upon the optimal UAV-sensor configuration derived in Section V-A (comprising four camera-equipped and

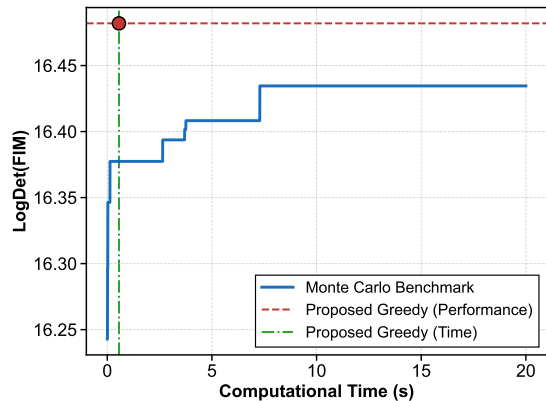


Fig. 7: Efficiency Comparison: Greedy vs. Monte Carlo method.

TABLE II: UAV Configuration Details

| UAV ID | Sensor | Azimuth ($^\circ$) | Pitch ($^\circ$) | Position (x, y, z) |
|--------|--------|----------------------|--------------------|----------------------|
| 1 | LiDAR | 40.0 | 160.0 | $(-7.2, -6.0, 3.4)$ |
| 2 | LiDAR | 130.0 | 20.0 | $(-6.0, 7.2, 3.4)$ |
| 3 | Camera | 0.0 | 160.0 | $(-9.4, -0.0, 3.4)$ |
| 4 | Camera | 100.0 | 20.0 | $(-1.6, 9.3, 3.4)$ |
| 5 | Camera | 50.0 | 160.0 | $(-6.0, -7.2, 3.4)$ |
| 6 | Camera | 140.0 | 160.0 | $(7.2, -6.0, 3.4)$ |

two LiDAR-equipped UAVs), we implement the formation optimization Alg. 2 described in Section IV-B to enhance spatial distribution while preserving perception accuracy. The optimization employs sector-constrained flipping operations (with $K = 8$ azimuthal sectors) to efficiently explore the equivalent formation space while maintaining computational tractability.

Fig. 9 shows the optimized formation configuration for aerial target tracking. The algorithm successfully transforms the initial heterogeneous UAV arrangement into a geometrically balanced formation that eliminates coverage blind spots while preserving the FIM determinant. This spatial reconfiguration demonstrates how equivalent geometric transformations can substantially improve operational effectiveness without compromising theoretical estimation bounds.

For ground-based SAR scenarios, physical terrain constraints preclude UAV deployment below the target plane.

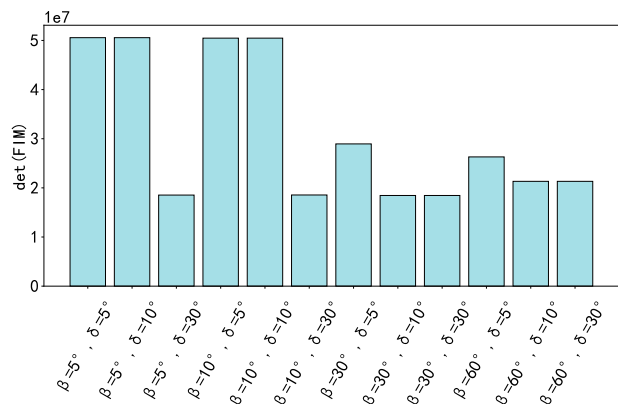


Fig. 8: Effect of Angular Discretization on Perception Performance

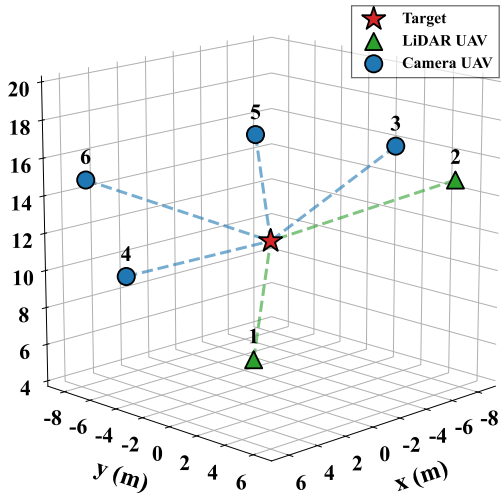


Fig. 9: Optimized formation configuration for air target.

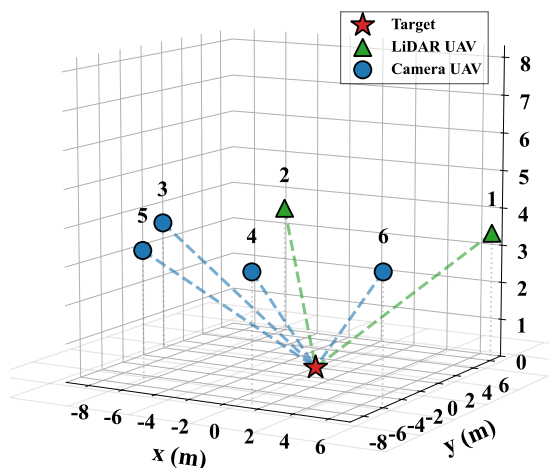


Fig. 10: Optimized formation configuration for ground target.

To address this practical limitation, we implement a Z-axis reflection transformation that repositions all UAVs to the feasible half-space while maintaining formation integrity. Although this constrained transformation introduces a marginal reduction in sensing accuracy, the resulting configuration (Fig. 10) achieves significantly enhanced field-of-view coverage and communication reliability compared to the initial arrangement.

Tab. III presents a comprehensive performance comparison between our optimized formation and a benchmark uniform enclosure configuration. For aerial targets, the optimized formation (Alg2) maintains the FIM log-determinant (Alg1) at 16.48 (superior to the uniform formation configuration's 16.124), while simultaneously achieving a 25.0% improvement in FOV coverage metric Γ (increasing from 21.99 (Alg1) to 27.49 (Alg2)). Most significantly, the average SINR increases by 104.2% (from 6.97 (Alg1) to 14.23 dB (Alg2)), with the minimum SINR rising from 1.78 dB (Alg1) to 11.51 dB

(Alg2), thereby ensuring reliable communication across the entire formation.

In ground target scenarios, the Z-axis reflection transformation yields a log-determinant of 16.414, marginally lower than the aerial target configuration but still exceeding the uniform configuration's 16.241. The FOV coverage metric reaches 27.49, surpassing the uniform configuration's 26.60, while the average SINR improves by 97.3% relative to the initial state (reaching 13.78 dB). Although slightly lower than the uniform configuration's 14.54 dB, this SINR level remains well within operational requirements for reliable data transmission.

TABLE III: Performance Comparison of Different Formations

| Metric | Alg1 | Alg2 (Air) | Alg2 (Gnd) | Bch. (Gnd) | Bch. (Air) |
|--------------------------|-------|------------|------------|------------|------------|
| $\log \det(\mathcal{F})$ | 16.48 | 16.48 | 16.41 | 16.24 | 16.12 |
| Γ | 21.99 | 27.49 | 27.49 | 26.60 | 26.60 |
| Avg. SINR | 6.97 | 14.23 | 13.78 | 14.54 | 14.92 |
| Min. SINR | 1.78 | 11.51 | 11.02 | 12.46 | 12.89 |

Note: Alg1 represents the formation configuration obtained from Alg. 1; Alg2 represents the formation configuration from Alg. 2 (Air/Ground); Bch.: Uniform formation as the benchmark (Ground/Air).

These results demonstrate that strategic formation geometry optimization can simultaneously enhance multiple performance metrics (i.e., coverage completeness, communication reliability, and preservation of sensing accuracy) validating our hypothesis that 3D spatial configuration represents a fundamental rather than incidental component in multimodal UAV swarm perception systems.

C. Flight Control Energy Efficiency

To validate the theoretical stability guarantees and energy efficiency of the proposed Lyapunov-based control framework presented in Section IV-C, we conducted comprehensive comparative simulations involving three distinct control strategies: (1) the proposed Lyapunov control law with logarithmic potential function, (2) a conventional Lyapunov control law employing quadratic potential function, and (3) the classical Artificial Potential Field (APF) method. The simulation scenario includes a swarm comprised by 6 UAVs ($M = 6$) with the optimal formation configuration derived from Section V-B serving as the target geometry. Each UAV was assigned a mass of $m_i = 1$ kg, and control gains were configured as $k_1 = 4$, $k_2 = 1.5$, $k_p = 10$. The UAV swarm tracked a time-varying reference trajectory $\mathbf{x}^{\text{des}}(t)$ generated by a target moving at a constant velocity of $v = [0.5, 0.3, 0.0]^T$ m/s. Among the baselines, the control law associated with the quadratic potential function is expressed as,

$$\mathbf{u}_i = \begin{cases} -k_1 \sum_{j \in \mathcal{M}_i} (\mathbf{e}_{ij}) - k_2 \mathbf{v}_i - k_p (\mathcal{P}_i - \mathcal{P}_i^{\text{des}}), & i = L, \\ -k_1 \sum_{j \in \mathcal{M}_i} (\mathbf{e}_{ij}) - k_2 \mathbf{v}_i, & i \neq L, \end{cases} \quad (43)$$

where L is the indicator of the leader UAV. For comparison, the classical APF method applies an attractive force that guides the UAV swarm to maintain the formation while tracking the target's reference trajectory. The attractive force is given as:

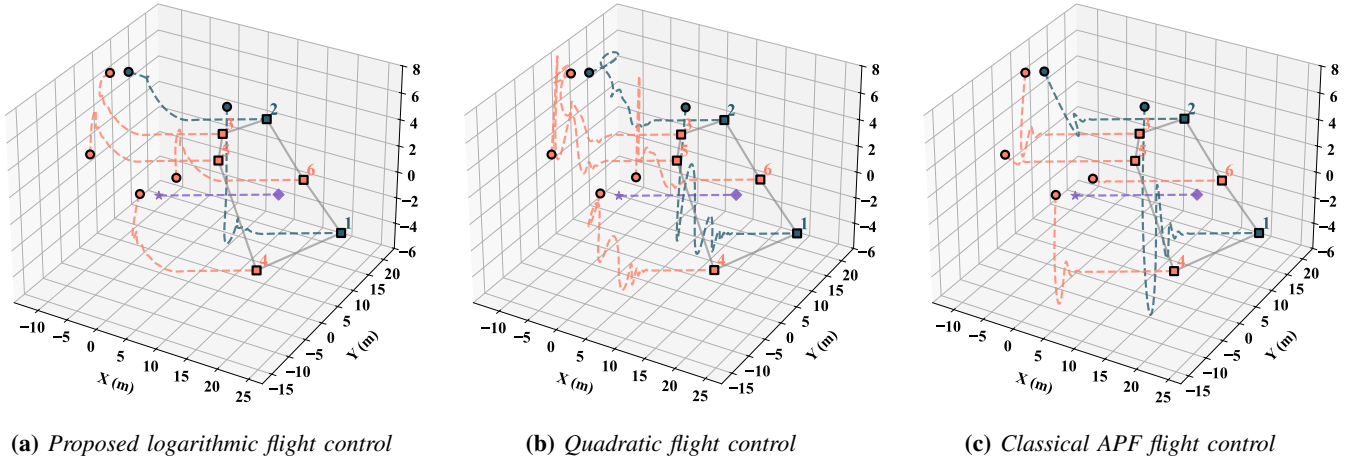


Fig. 11: 3D Trajectory Comparison of Three Control Methods

$$\mathbf{F}_{\text{att},i} = -k_a(\mathcal{P}_i - \mathcal{P}_i^*), \quad (44)$$

Furthermore, a repulsive force is generated from all neighboring UAVs for maintaining safe separation, which is,

$$\mathbf{F}_{\text{rep},i} = \sum_{j \in \mathcal{M}_i} k_r \left(\frac{1}{\|\mathcal{P}_{ij}\|} - \frac{1}{d_0} \right) \frac{\mathcal{P}_{ij}}{\|\mathcal{P}_{ij}\|^3}, \quad \|\mathcal{P}_{ij}\| < d_0, \quad (45)$$

where $\mathcal{P}_{ij} = \mathcal{P}_i - \mathcal{P}_j$, d_0 is the safe separation distance. Therefore, the APF control input is:

$$\mathbf{u}_i = \mathbf{F}_{\text{att},i} + \mathbf{F}_{\text{rep},i} - k_2 \mathbf{v}_i. \quad (46)$$

TABLE IV: Performance Comparison of Flight Control

| Metric | Logarithmic | Quadratic | Classical APF |
|--------------------------|-------------|-----------|---------------|
| Avg. Distance (m) | 15.62 | 29.60 | 19.40 |
| Avg. Velocity Err. | 0.678 | 1.736 | 0.883 |
| Max. Velocity Err. | 7.666 | 8.907 | 10.865 |
| Avg. Final Pos. Err. (m) | 0.056 | 0.085 | 0.107 |

Tab. IV summarizes the quantitative performance metrics during the formation transition from initial to steady-state configuration. The logarithmic potential-based controller shows superior performance across all evaluated metrics. Specifically, it achieves the shortest average travel distance of 15.62 m, representing a 47.2% reduction compared to the quadratic controller (29.60 m) and a 19.5% improvement relative to the classical APF method (19.40 m). This distance minimization directly translates to reduced energy consumption, as flight energy expenditure is predominantly proportional to path length in UAV operations.

The velocity profile analysis further confirms the energy-efficient characteristics of our approach. The logarithmic controller exhibits an average velocity error of 0.678 m/s and maximum velocity error of 7.666 m/s, substantially lower than both the quadratic controller (1.736 m/s and 8.907 m/s) and classical APF method (0.883 m/s and 10.865 m/s). These reductions of 61.0% and 13.9% in average velocity error compared to the quadratic controller, and 23.2% and 29.4% relative

to the APF method, indicate significantly smoother motion profiles with fewer aggressive maneuvers. The final position error of 0.056 m achieved by the logarithmic controller also represents a 34.1% and 47.7% improvement over the quadratic and APF methods, respectively, confirming its superior steady-state accuracy.

Fig. 11 illustrates the 3D trajectory evolution under each control strategy. The logarithmic potential-based approach (Fig. 11a) exhibits notably smooth convergence without overshoot or oscillatory behavior. In contrast, both the quadratic potential method (Fig. 11b) and classical APF approach (Fig. 11c) demonstrate pronounced oscillations during the transient phase, particularly when correcting large initial formation errors. These oscillations necessitate additional corrective maneuvers that increase energy consumption and reduce flight stability.

The position error dynamics in Fig. 12 provide further evidence of the proposed controller's advantages. The logarithmic potential formulation achieves monotonic error reduction across all three spatial dimensions with minimal fluctuations, whereas both comparative methods exhibit significant oscillatory behavior before reaching steady state. While maintaining comparable convergence rates to the quadratic controller, our approach eliminates the high-frequency oscillations that characterize conventional methods during the transient phase. This smooth error evolution directly contributes to reduced control effort, as evidenced by the lower maximum velocity error, and consequently minimizes energy-intensive maneuvers.

Theoretical analysis from Section IV-C established global asymptotic stability through the Lyapunov function's negative semi-definite derivative (Eq. (42)). The experimental results validate this theoretical guarantee while demonstrating the practical energy efficiency benefits of the logarithmic potential field. By bounding control authority during large formation errors through the logarithmic term $\ln(1 + \|\mathbf{e}_{ij}\|^2)$, the controller prevents excessive corrective actions that would otherwise increase energy consumption. This design principle achieves the optimal balance between rapid convergence and energy conservation that is essential for extended UAV swarm

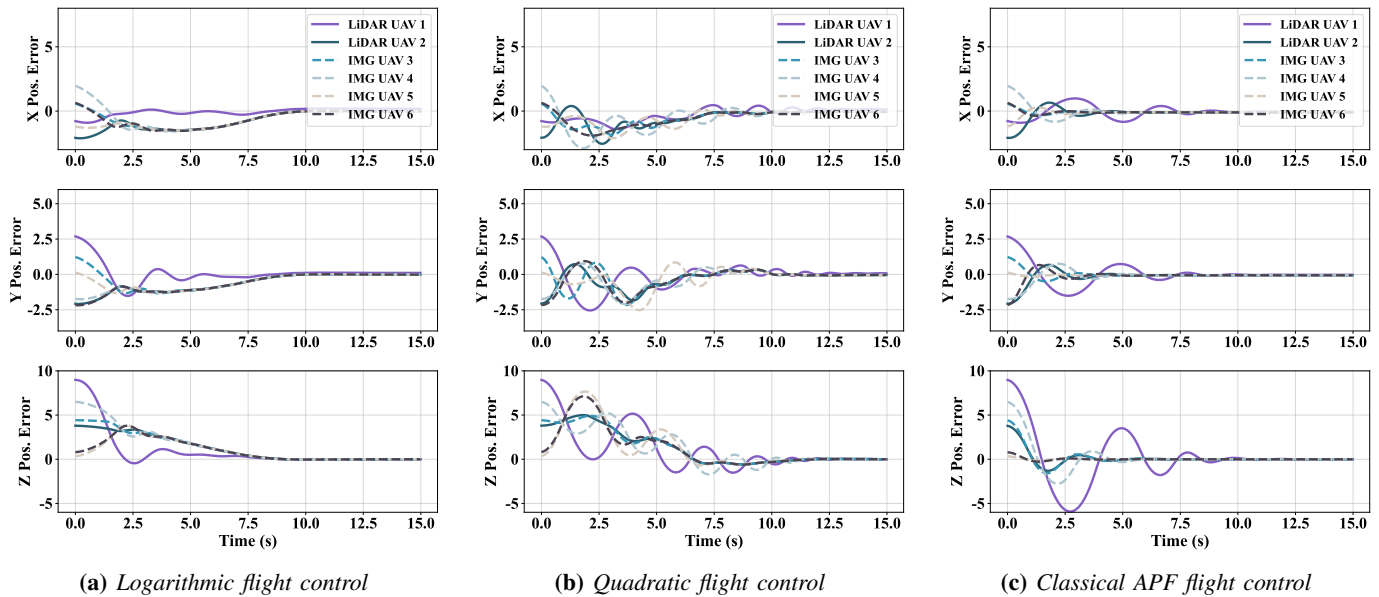


Fig. 12: 3D Position Error Distribution of Three Flight Control Methods

operations in SAR scenarios.

These results confirm that the proposed Lyapunov-based control law with logarithmic potential function significantly outperforms conventional approaches in trajectory smoothness, convergence accuracy, and energy efficiency. Its ability to maintain precise formation geometry while minimizing unnecessary maneuvers makes it particularly suitable for real-world UAV swarm applications where energy constraints and operational stability are critical considerations.

VI. CONCLUSION

In this paper, we investigated the problem of UAV swarm cooperative perception with formation geometry as a fundamental design element. We proposed an FID-based framework that jointly optimizes system performance with three key components. The first is a submodular greedy algorithm for UAV-sensor allocation with theoretical $(1 - 1/e)$ -approximation guarantees. The second is an equivalent formation transformation strategy that enhances FOV coverage by 25.0% while improving communication SINR by 104.2% without compromising sensing accuracy. The third is a Lyapunov-stable flight controller with logarithmic potential fields that reduces travel distance by 47.2% compared to conventional approaches. Our experimental validation demonstrates that strategic spatial configuration significantly enhances multi-modal perception performance under practical constraints of communication interference, energy limitations, and hardware budgets. The framework bridges a critical gap between theoretical information bounds and operational requirements in search and rescue scenarios. This formation-aware paradigm can provide guidelines for UAV swarm systems where geometric configuration, sensor complementarity, and communication constraints are optimized as an integrated whole rather than isolated components.

REFERENCES

- [1] M. Mozaffari, W. Saad, M. Bennis, Y.-H. Nam, and M. Debbah, "A tutorial on uavs for wireless networks: Applications, challenges, and open problems," *IEEE Communications Surveys & Tutorials*, vol. 21, no. 3, pp. 2334–2360, 2019.
- [2] S. Lee, D. Har, and D. Kum, "Drone-assisted disaster management: Finding victims via infrared camera and lidar sensor fusion," in *2016 3rd Asia-Pacific World Congress on Computer Science and Engineering (APWC on CSE)*, 2016, pp. 84–89.
- [3] N. Souli, P. Kardaras, P. Kolios, and G. Ellinas, "A joint rogue drone detection and tracking fusing doa and passive radar measurements," in *2024 International Conference on Unmanned Aircraft Systems (ICUAS)*, 2024, pp. 1200–1207.
- [4] R. Tallamraju, E. Price, R. Ludwig, K. Karlapalem, H. H. Bühlhoff, M. J. Black, and A. Ahmad, "Active perception based formation control for multiple aerial vehicles," *IEEE Robotics and Automation Letters*, vol. 4, no. 4, pp. 4491–4498, 2019.
- [5] J. Wu, D. Li, Y. Yu, L. Gao, J. Wu, and G. Han, "An attention mechanism and adaptive accuracy triple-dependent maddpg formation control method for hybrid uavs," *IEEE Transactions on Intelligent Transportation Systems*, vol. 25, no. 9, pp. 11 648–11 663, 2024.
- [6] T. Gavin, S. Lacroix, and M. Bronz, "Multi-agent reinforcement learning based drone guidance for n-view triangulation," in *2024 International Conference on Unmanned Aircraft Systems (ICUAS)*, 2024, pp. 578–585.
- [7] D. Liu, B. Fei, W. Bao, X. Zhu, and X. Li, "Dawn: Dynamic task planning of multi-uav with two-layer optimization mechanism in uncertain environments," *IEEE Internet of Things Journal*, vol. 11, no. 23, pp. 37 813–37 830, 2024.
- [8] Q. Zhang, Y. Luo, H. Jiang, and K. Zhang, "Aerial edge computing: A survey," *IEEE Internet of Things Journal*, vol. 10, no. 16, pp. 14 357–14 374, 2023.
- [9] T. Lou, Y. Wang, Z. Yue, and L. Zhao, "Multi-uav collaborative trajectory planning for 3d terrain based on cs-gjo algorithm," *Complex System Modeling and Simulation*, vol. 4, no. 3, pp. 274–291, 2024.
- [10] B. Zhou, J. Pan, F. Gao, and S. Shen, "Raptor: Robust and perception-aware trajectory replanning for quadrotor fast flight," *IEEE Transactions on Robotics*, vol. 37, no. 6, pp. 1992–2009, 2021.
- [11] W. Lee, H. Bang, and H. Leeghim, "Cooperative localization between small uavs using a combination of heterogeneous sensors," *Aerospace Science and Technology*, vol. 27, no. 1, pp. 105–111, 2013. [Online]. Available: <https://www.sciencedirect.com/science/article/pii/S1270963812001101>
- [12] A. Kurt, N. Saputro, K. Akkaya, and A. S. Uluagac, "Distributed connectivity maintenance in swarm of drones during post-disaster transportation applications," *IEEE Transactions on Intelligent Transportation Systems*, vol. 22, no. 9, pp. 6061–6073, 2021.

- [13] K. Panwar, G. Fatima, and P. Babu, "Optimal Sensor Placement for Hybrid Source Localization Using Fused TOA-RSS-AOA Measurements," *IEEE Transactions on Aerospace and Electronic Systems*, pp. 1–15, 2022.
- [14] S. Zhao, B. M. Chen, and T. H. Lee, "Optimal Sensor Placement for Target Localization and Tracking in 2D and 3D," *International Journal of Control*, vol. 86, no. 10, pp. 1687–1704, Oct. 2013.
- [15] M. Lyu, Y. Zhao, C. Huang, and H. Huang, "Unmanned Aerial Vehicles for Search and Rescue: A Survey," *Remote Sensing*, vol. 15, no. 13, p. 3266, Jun. 2023.
- [16] J. Li, B. Yang, W. Wu, W. Dai, C. Chen, X. Zou, and M. Tian, "3D MOBILE MAPPING WITH A LOW COST UAV SYSTEM," *The International Archives of the Photogrammetry, Remote Sensing and Spatial Information Sciences*, vol. XLII-2/W8, pp. 127–132, Nov. 2017.
- [17] M. Tavakol Sadrabadi, J. Peiro, M. S. Innocente, and G. Rein, "Conceptual Design of a Wildfire Emergency Response System Empowered by Swarms of Unmanned Aerial Vehicles," 2024.
- [18] L. Xing, X. Fan, Y. Dong, Z. Xiong, L. Xing, Y. Yang, H. Bai, and C. Zhou, "Multi-UAV cooperative system for search and rescue based on YOLOv5," *International Journal of Disaster Risk Reduction*, vol. 76, p. 102972, Jun. 2022.
- [19] H. Zeng, L. Tong, and X. Xia, "Multi-UAV Cooperative Coverage Search for Various Regions Based on Differential Evolution Algorithm," *Biomimetics*, vol. 9, no. 7, p. 384, Jun. 2024.
- [20] L. Yang, Y. Hao, J. Xu, and M. Li, "Multi-UAV Collaborative Target Search Method in Unknown Dynamic Environment," *Sensors*, vol. 24, no. 23, p. 7639, Nov. 2024.
- [21] Y.-C. Liu, J. Tian, N. Glaser, and Z. Kira, "When2com: Multi-Agent Perception via Communication Graph Grouping," in *2020 IEEE/CVF Conference on Computer Vision and Pattern Recognition (CVPR)*. Seattle, WA, USA: IEEE, Jun. 2020, pp. 4105–4114.
- [22] T.-H. Wang, S. Manivasagam, M. Liang, B. Yang, W. Zeng, J. Tu, and R. Urtasun, "V2VNet: Vehicle-to-Vehicle Communication for Joint Perception and Prediction," Aug. 2020.
- [23] R. Xu, H. Xiang, Z. Tu, X. Xia, M.-H. Yang, and J. Ma, "V2X-ViT: Vehicle-to-Everything Cooperative Perception with Vision Transformer," Aug. 2022.
- [24] V. Semenyuk, I. Kurmashev, A. Lupidi, D. Alyoshin, L. Kurmasheva, and A. Cantelli-Forti, "Advances in UAV detection: Integrating multi-sensor systems and AI for enhanced accuracy and efficiency," *International Journal of Critical Infrastructure Protection*, vol. 49, p. 100744, Jul. 2025.
- [25] P. Tian, P. Cheng, Y. Wang, Z. Wang, Z. Wang, M. Yan, X. Yang, and X. Sun, "UCDNet: Multi-UAV Collaborative 3D Object Detection Network by Reliable Feature Mapping," Jun. 2024.
- [26] D. Qiao and F. Zulkernine, "CoBEVFusion: Cooperative Perception with LiDAR-Camera Bird's-Eye View Fusion," Oct. 2023.
- [27] S. Bultmann, J. Quenzel, and S. Behnke, "Real-time multi-modal semantic fusion on unmanned aerial vehicles with label propagation for cross-domain adaptation," *Robotics and Autonomous Systems*, vol. 159, p. 104286, Jan. 2023.
- [28] T. Feng, X. Wang, F. Han, L. Zhang, and W. Zhu, "U2Udata: A Large-scale Cooperative Perception Dataset for Swarm UAVs Autonomous Flight," in *Proceedings of the 32nd ACM International Conference on Multimedia*, Oct. 2024, pp. 7600–7608.
- [29] H.-A. Hung, H.-H. Hsu, and T.-H. Cheng, "Optimal Sensing for Tracking Task by Heterogeneous Multi-UAV Systems," *IEEE Transactions on Control Systems Technology*, vol. 32, no. 1, pp. 282–289, Jan. 2024.
- [30] N. Sahu, L. Wu, P. Babu, B. S. M. R., and B. Ottersten, "Optimal Sensor Placement for Source Localization: A Unified ADMM Approach," *IEEE Transactions on Vehicular Technology*, vol. 71, no. 4, pp. 4359–4372, Apr. 2022.
- [31] K. Nakai, K. Yamada, T. Nagata, Y. Saito, and T. Nonomura, "Effect of Objective Function on Data-Driven Greedy Sparse Sensor Optimization," *IEEE Access*, vol. 9, pp. 46 731–46 743, 2021.
- [32] Z. Wang, R. Liu, Q. Liu, J. S. Thompson, and M. Kadoch, "Energy-Efficient Data Collection and Device Positioning in UAV-Assisted IoT," vol. 7, no. 2, pp. 1122–1139. [Online]. Available: <https://ieeexplore.ieee.org/document/8894454/>
- [33] F. Morbidi and G. L. Mariottini, "Active target tracking and cooperative localization for teams of aerial vehicles," *IEEE Transactions on Control Systems Technology*, vol. 21, no. 5, pp. 1694–1707, 2013.
- [34] K. Yamada, Y. Saito, K. Nankai, T. Nonomura, K. Asai, and D. Tsubakino, "Fast Greedy Optimization of Sensor Selection in Measurement with Correlated Noise," vol. 158, p. 107619. [Online]. Available: <http://arxiv.org/abs/1912.01776>
- [35] J. LaSalle, "Some extensions of liapunov's second method," *IRE Transactions on circuit theory*, vol. 7, no. 4, pp. 520–527, 1960.